



PAST

## Design Concepts and Overview

Sun Sensors (OSIRIS)

Felix Abbott, Indi Malinton

Perth Aerospace Student Team  
Attitude Determination and Control Systems

June 2025

## Contents

<b>1</b>	<b>Introduction</b>	<b>2</b>
1.1	Background . . . . .	2
1.2	Project Scope . . . . .	2
<b>2</b>	<b>Requirements</b>	<b>2</b>
<b>3</b>	<b>Timeline</b>	<b>2</b>
3.1	December 2024: Foundational Research . . . . .	2
3.2	January 2025: OSIRISv1 Design . . . . .	2
3.3	February 2025: Fabrication and Assembly of OSIRISv1 . . . . .	2
3.4	March 2025: Testing OSIRISv1 and Iterating Design . . . . .	3
3.5	April 2025: Finalising and Ordering OSIRISv2 . . . . .	3
3.6	May/June 2025: Rigorous Testing of OSIRISv2 . . . . .	3
<b>4</b>	<b>Test Board (v1)</b>	<b>3</b>
4.1	Background . . . . .	3
4.2	Component Selection . . . . .	3
4.3	Test Board PCB Design . . . . .	6
4.4	Testing . . . . .	6
4.5	Review . . . . .	7
4.6	Achievements . . . . .	7
4.7	Challenges and Lessons Learned . . . . .	8
4.8	Reflection . . . . .	8
<b>5</b>	<b>Sun Sensor Prototype (v2)</b>	<b>8</b>
5.1	Background . . . . .	8
5.2	Photodiode Module Schematic . . . . .	8
5.2.1	Transimpedance Amplifier Configuration . . . . .	9
5.2.2	Component Value Calculations . . . . .	9
5.2.3	Circuit Simulation . . . . .	9
5.3	PCB Design . . . . .	10
5.4	Fabrication . . . . .	10
5.5	Sun Vector Determination Algorithm . . . . .	11
5.6	Testing . . . . .	11
5.6.1	Experimental Setup . . . . .	12
5.6.2	Calibration . . . . .	13
5.6.3	Interpreting Data . . . . .	14
5.6.4	Gathering Data . . . . .	14
5.7	Analysing Results . . . . .	17
5.7.1	Uncertainties . . . . .	19
<b>6</b>	<b>Github Resources</b>	<b>20</b>

# 1 Introduction

## 1.1 Background

Sun sensors are used to determine the sun vector in the CubeSat's body-fixed frame. The sun vector can then be used in attitude determination algorithms to parameterise the CubeSat's orientation relative to the Earth.

There are three main categories of sun sensors:

- **Fine Analogue Sun Sensors:** These allow incident light to enter through a small window onto a photodiode with various quadrants or a position-sensitive device. Currents in independent photodiodes allow for the determination of the sun vector in two axes.
- **Coarse Sun Sensors:** These measure incident light without windows or projections using photodiodes. Photocurrent is proportional to the cosine of the angle between the incident light and the normal vector. At least three photodiodes must be exposed to sunlight to obtain the sun vector.
- **Digital Sun Sensors:** These use photosensitive units made up of thousands to millions of light-sensitive pixels below a window. They offer higher sensitivity and accuracy but are very expensive.

This project aims to develop Coarse Sun Sensors due to cost constraints and component availability.

## 1.2 Project Scope

This project aims to design, develop, and test a Coarse Sun Sensor (CSS), integrating electronic and computational subsystems. The focus is on assembling a prototype that meets performance criteria while adhering to size, power consumption, and operating environment constraints.

OSIRISv1 is the test board component for the project, used for testing and selecting the photodiode (PD) for the High-Altitude Balloon (HAB).

# 2 Requirements

The overarching objective of this project is to develop a viable and functioning prototype CSS that:

- Computes the direction of the sun vector in the CubeSat's body-fixed frame to a low degree of uncertainty ( $\pm 10^\circ$ ).
- Identifies the CubeSat's orientation relative to the sun and communicates adjustments to a terminal and/or microcontroller.

# 3 Timeline

## 3.1 December 2024: Foundational Research

- Review scientific literature and technical datasheets.
- Compare photodiodes based on spectral sensitivity, angular response, and linearity.
- Explore TIA configurations for low-current photodiode applications.
- Shortlist candidate components for prototyping.

## 3.2 January 2025: OSIRISv1 Design

- Design board layout for four photodiodes with independent TIAs.
- Calculate component values for each TIA.
- Prepare board for modular testing.
- Review annotated schematics and layouts.

## 3.3 February 2025: Fabrication and Assembly of OSIRISv1

- Submit .gerber files and order components.
- Develop microcontroller code to read ADC values.

### 3.4 March 2025: Testing OSIRISv1 and Iterating Design

- Collect comparative data under varying lighting conditions.
- Identify and address design issues.
- Use findings to inform OSIRISv2 design.

### 3.5 April 2025: Finalising and Ordering OSIRISv2

- Finalise OSIRISv2 design.
- Enhance design with improvements (e.g., voltage regulation).
- Order PCB and parts for fabrication.

### 3.6 May/June 2025: Rigorous Testing of OSIRISv2

- Perform controlled environment testing.
- Conduct angular response and stability tests.
- Compare performance with theoretical models.

## 4 Test Board (v1)

### 4.1 Background

The OSIRIS test board (v1) aims at determining the most effective photodiode of the four picked from the research stage. After a few weeks of understanding sun sensors, examining potential photodiodes and components, four photodiodes were chosen to be placed on the test board. Some background on photodiodes is provided below. Photodiodes are semi-conductor devices with a P-N junction that convert the energy from incident photons (light) into electrical current. [This video](#) is a good explanation of how photodiodes work. To operate as a light-sensing device, photodiodes must be configured in zero or reverse bias. As shown in the voltage-current curve below, the photocurrent generated by photodiodes is negative. This means conventional current flows from the anode to cathode (opposite of diode direction). They have a linear response to the amount illuminated onto them.

Photocurrent depends on:

- **Angle of Incidence:** The most photocurrent will be produced when the source is directly above the PD (when the source's vector is perpendicular to the PD). The magnitude of this can be related by  $I = I_M \cos\theta$ , where  $I_M$  is the maximum photocurrent and  $\theta$  the angle between the PD and vector (this is called the Lambertian Response). It is usually independent of this when  $\theta < 30^\circ$ .
- **Relative Spectral Sensitivity:** At certain wavelengths, photodiodes will produce different results. Usually in datasheets this will be depicted in the Relative Spectral Sensitivity. This shows how effectively the photodiode will operate at different wavelengths. For sun sensors, we want a high % at 500nm. You can see an example on the right.

Photodiodes can be modelled as a current source. A TIA in a transimpedance amplifier configuration is required to convert the input current source into a voltage output that can be read using an ADC pin of a microcontroller.

### 4.2 Component Selection

Selected photodiodes for OSIRISv1:

- Photodiode A: [OSRAM SFH\\_2240](#)
- Photodiode B: [OSRAM SFH\\_2240\\_A01](#)
- Photodiode C: [VEMD5510FX01](#)
- Photodiode D: [SFH\\_2430\\_Z](#)

The following Op Amp was used [LM321LVIDCKR](#). This [Photodiode Amplifier Reference Design](#) from Texas Instruments was used to calculate the component values for the transimpedance amplifier. Resistors, capacitors and [LEDs](#) used the 0603 surface mount.

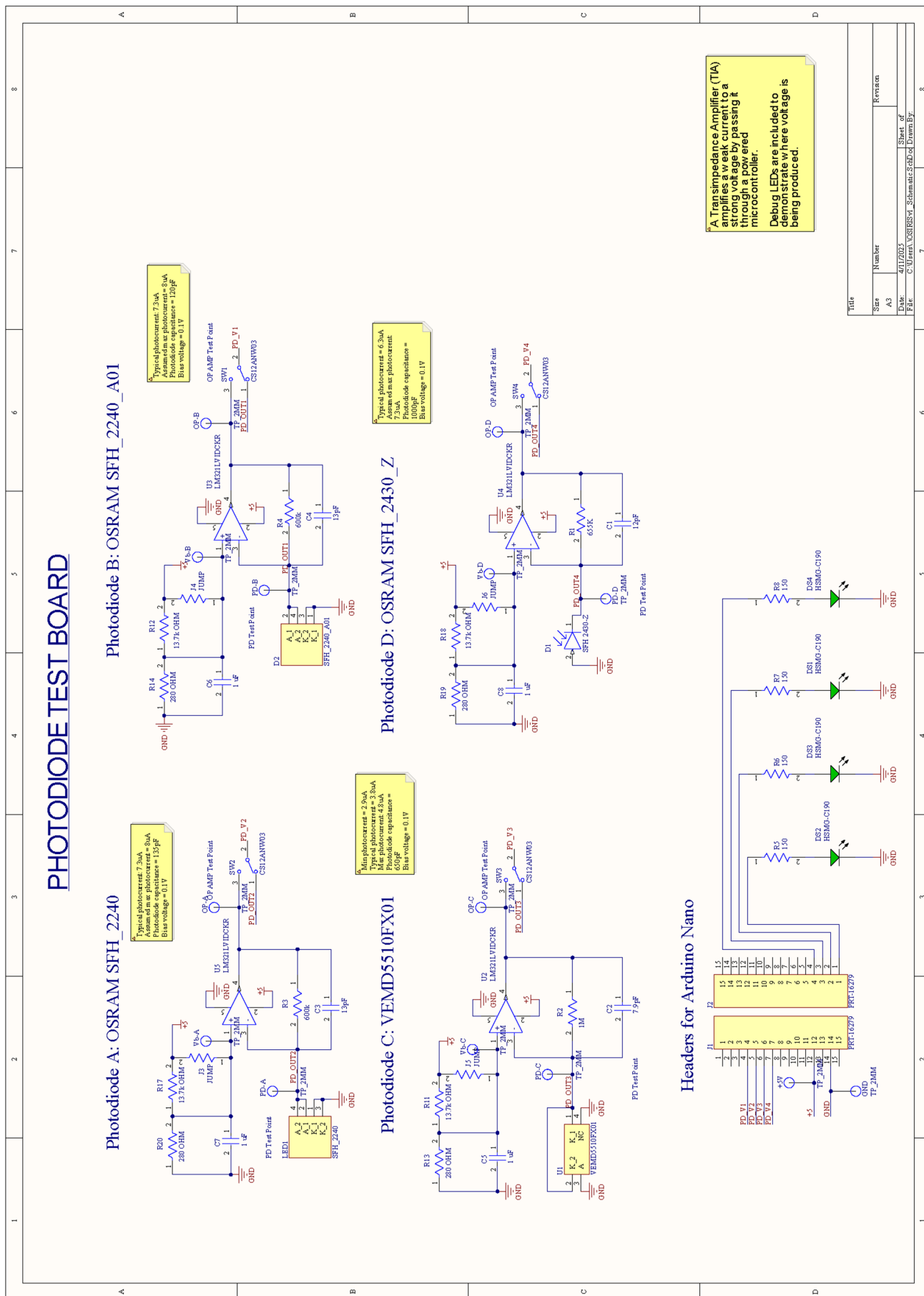
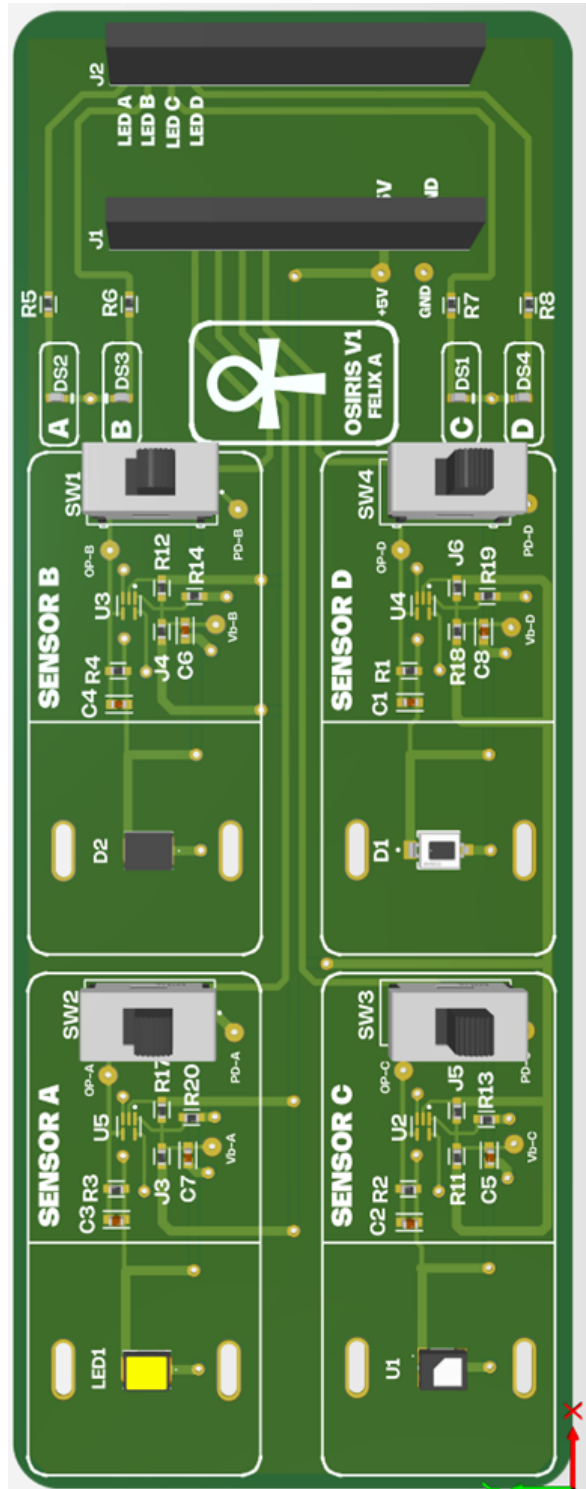
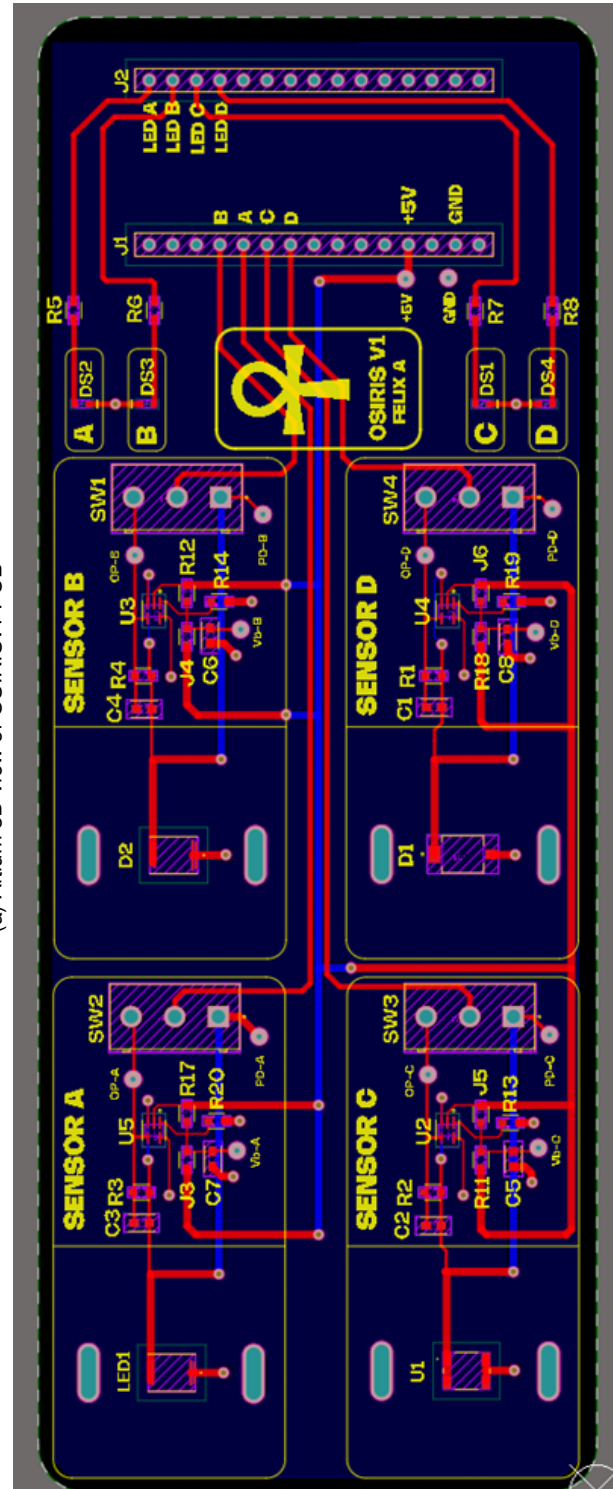


Figure 1: Altium schematic of OSIRSV1 Test Board



(a) Altium 3D view of OSIRISv1 PCB



(b) Altium wire view of OSIRISv1 PCB

Figure 2: Altium PCB visualizations of OSIRISv1 (3D and wire views)

### 4.3 Test Board PCB Design

### 4.4 Testing

Each photodiode was connected to a TIA with its respective component values, however, due to a design fault, the TIAs were not functional, so, the ADC values were read directly from the photodiodes themselves (each photodiode was fortunately connected to the feedback resistor from the TIA design, so a voltage was read, not the current). To mitigate this issue, the following formula was implemented.

$$\psi = \frac{1}{IR} \left( \frac{5A}{1023} - B \right)$$

Where:

- $A$ : ADC value
- $B$ : Baseline reading
- $IR$ : Peak current and resistor product

The bracketed equation adjusts each reading so that they all have a minimum of zero, and the scalar outside accounts for the different component values. Altogether, the output,  $\psi$ , is a unitless variable which represents the normalised readings from each photodiode.

Placing OSIRISv1 in different environments, the results were gathered and collated to evaluate the best performing photodiode. Baseline tests were gathered to determine the minimum reading in a near-pitch black environment, and because of the design fault, the ADC values were scaled to account for the different current outputs and resistors attached.

Testing in varied environments yielded the following results (unitless values):

	Photodiode A	Photodiode B	Photodiode C	Photodiode D
Baseline (<5 Lux)	$0 \pm 8$	$0 \pm 8$	$0 \pm 8$	$0 \pm 8$
Shaded Light (357 Lux)	$39 \pm 8$	$53 \pm 8$	$62 \pm 8$	$19 \pm 8$
Direct Sunlight (25.7k Lux)	$67 \pm 8$	$85 \pm 8$	$93 \pm 8$	$7 \pm 8$
Angled Sunlight (25.7k Lux)	$62 \pm 8$	$89 \pm 8$	$96 \pm 8$	$10 \pm 8$
Studio Light (1200 Lux)	$50 \pm 8$	$64 \pm 8$	$73 \pm 8$	$24 \pm 8$

Table 1: Summary of finding from OSIRISv1 testing. Note that the values are unitless and are not representative of the voltage or current. Each reading has an uncertainty of 8 from the baseline test.

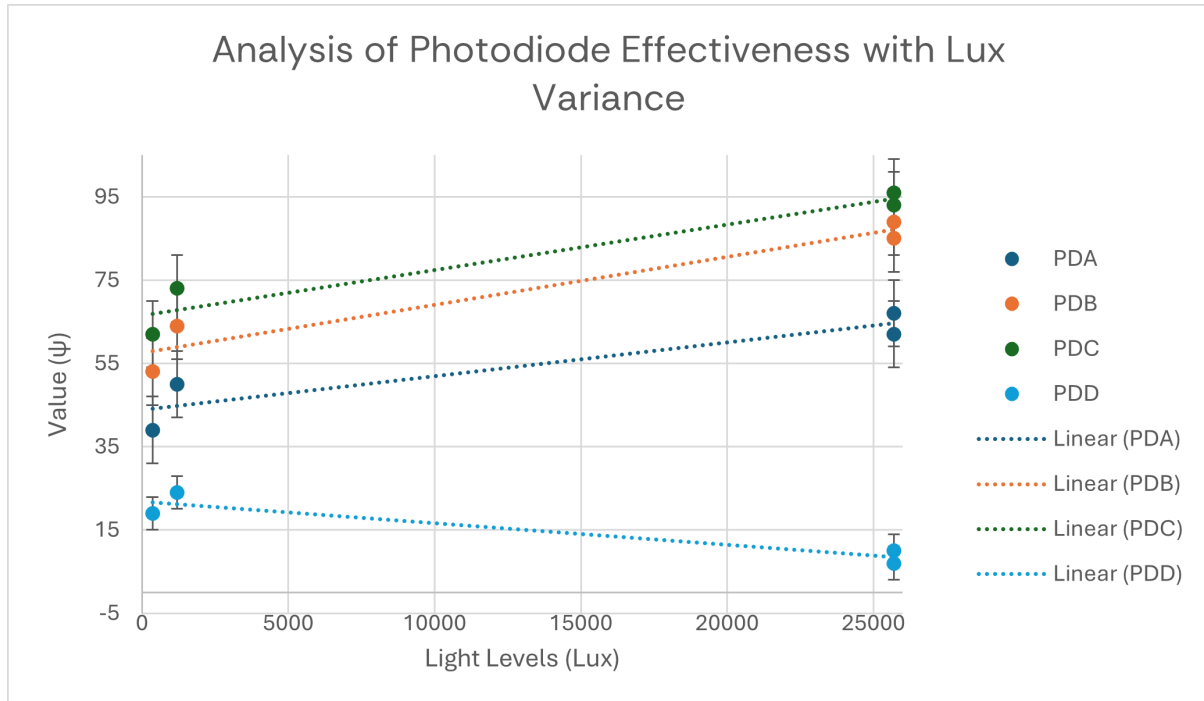


Figure 3: Scatterplot of findings from OSIRISv1 testing (value over lux). Note that the values are unitless and are not representative of the voltage or current. To improve linear regression on the data points, the baseline has been excluded. An uncertainty of 8 is included on each data point. Photodiode A is green, B is orange, navy is C, light-blue is D.

It must be noted that the TIA design fault (5V and GND terminals were mixed up) made it very difficult to know which photodiode performed best, since no photodiode was tested under universal conditions (different resistor values and current curves could not be accurately accounted for by a linear scale because of the non-linear nature of the intensity function). Additionally, there was an issue soldering Photodiode D onto the board which may account for some error.

Although it is not evident which photodiode performed the best (within uncertainty), photodiode C (VEMD5510FX01) proved to be the tied most effective at outputting a current proportional to sunlight, and most effective according to the data sheet. Moreover, it was recommended by Robert Howie (Spacecraft Project UC). Despite this, photodiode B performed as well as photodiode C within uncertainty. Should there be any future OSIRIS projects, both B and C must be taken into consideration.

## 4.5 Review

The OSIRISv1 test board served as a crucial first step in evaluating and selecting the most suitable photodiode for future sun-sensing applications. While it ultimately fell short of providing definitive conclusions due to a design oversight, the board still yielded valuable insights and experience in both hardware development and testing methodology.

## 4.6 Achievements

Despite the non-functional transimpedance amplifiers (TIAs) caused by the reversed 5V and GND terminals, the board allowed direct voltage readings from the photodiodes through the feedback resistors. This fallback, although less precise than a full TIA output, enabled relative comparisons between the photodiodes under various lighting conditions using a normalised output variable,  $\psi$ . Testing spanned a range of realistic lighting environments, including shaded conditions, studio lighting, and direct sunlight.

Photodiodes B and C emerged as the strongest candidates. Photodiode C (VEMD5510FX01) aligned well with theoretical expectations and datasheet specifications, showing consistently high output across all environments. Photodiode B (SFH 2240 A01) performed comparably within uncertainty margins, highlighting its potential as a viable alternative. Additionally, the board reaffirmed the need for consistent and precise design execution, particularly when working with analogue sensor circuitry.

## 4.7 Challenges and Lessons Learned

The biggest limitation of OSIRISv1 was the TIA circuit design flaw, which significantly reduced the test board's intended functionality. With the TIA stage non-functional, precise voltage conversion and signal amplification were compromised, meaning results had to be normalised through mathematical approximations. This introduced inherent uncertainty and limited the accuracy of inter-diode comparisons.

Soldering issues with Photodiode D and the variability in component values (especially resistors in the TIA configuration) further impacted the reliability of the results. Future iterations must prioritise more rigorous schematic verification, especially in power supply routing and signal path integrity.

Another lesson learned was the importance of modular design. Had the TIAs been independently testable or socketed, troubleshooting and replacement would have been more feasible without scrapping the board. Additionally, more thorough prototyping or simulation of the TIA design might have caught the power pin issue before fabrication.

## 4.8 Reflection

OSIRISv1 provided valuable insights despite its flaws. Key takeaways include ensuring proper power routing, modular testing design, and consistent component values.

# 5 Sun Sensor Prototype (v2)

## 5.1 Background

OSIRISv2 aims at developing a functioning sun sensor prototype that can effectively determine the position of a light source within the agreed degree of uncertainty. Using photodiode sun sensor modules (disconnected from the microcontroller board), we can construct testing rigs and implement sun vector acquisition algorithms to compute the position of light sources in real-time.

### OSIRISv2 Block Diagram

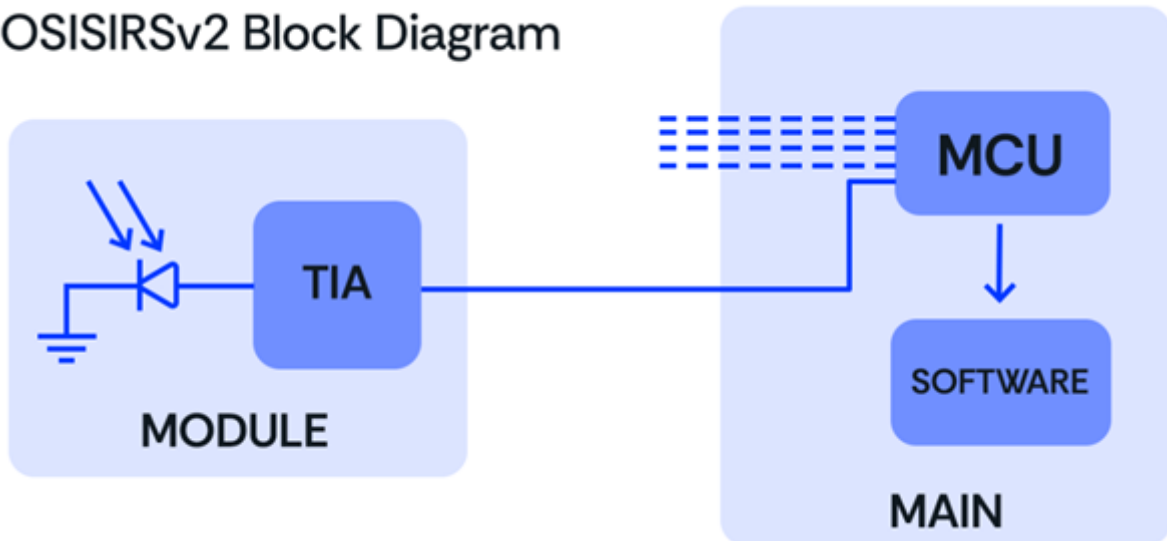


Figure 4: Block diagram of OSIRISv2 functionality

## 5.2 Photodiode Module Schematic

This [Photodiode Amplifier Reference Design](#) from Texas Instruments was used to calculate the component values for the transimpedance amplifier. The schematic is shown below. *Please note that the photodiode in the following schematic is incorrect and is in the wrong orientation. The cathode should go to ground and the anode should go to the TIA.*

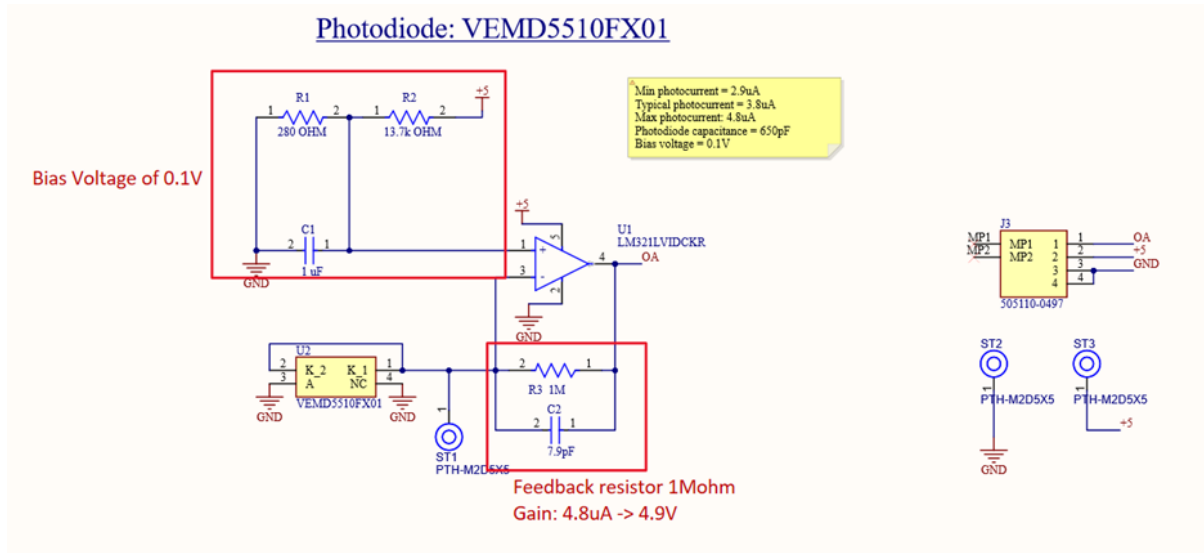


Figure 5: Altium schematic of the OSIRISv2 module board.

The module simply consists of a photodiode, a TIA, and a 4 pin FPC connector. Unlike OSIRISv1, the sensor board module is disconnected from the microcontroller and can be fitted to a testing rig due to the small size.

### 5.2.1 Transimpedance Amplifier Configuration

- Photodiode's cathode is connected to the inverting input (photocurrent flows from anode to cathode).
- A bias voltage of 0.1V is supplied to the non-inverting input. This is because in an absence of any photocurrent, the TIA output will saturate near its negative power supply and cause a delay in the amplifier's response to the input signal.
- The voltage to current gain is based on the value of the feedback resistor. Our design initially used a feedback resistor value of 1Mohm to amplify the max photocurrent (4.8uA) to 4.9V.

### 5.2.2 Component Value Calculations

The capacitance and max current of the photodiode, as listed in the datasheet, is  $C_J = 120\text{pF}$  and  $I_M = 4.8\mu\text{A}$ . We find that the feedback resistor must have a value of

$$R_f = \frac{V_M - V_{IN}}{I_M} = \frac{4.9 - 0.1}{4.8 \times 10^{-6}} = 1 \times 10^6 \Omega$$

And the feedback capacitor,

$$C_f = \frac{1}{2\pi R_f f} = \frac{1}{2\pi \times 1 \times 10^6 \times 20 \times 10^3} = 7.96 \times 10^{-12}$$

The capacitor for the biased filter must have a value of  $C_b = 1 \times 10^{(-6)}$ , and the ratio of resistors must be equivalent to

$$\frac{R_1}{R_2} = \frac{V_{CC} - V_{REF}}{V_{REF}} = \frac{5 - 0.1}{0.1} = 49$$

So, we chose values of  $R_1 = 13.7 \times 10^3 \Omega$  and  $R_2 = 280\Omega$ , whose ratio is 49.

### 5.2.3 Circuit Simulation

The circuit was modelled in Falstad and produced the expected results.

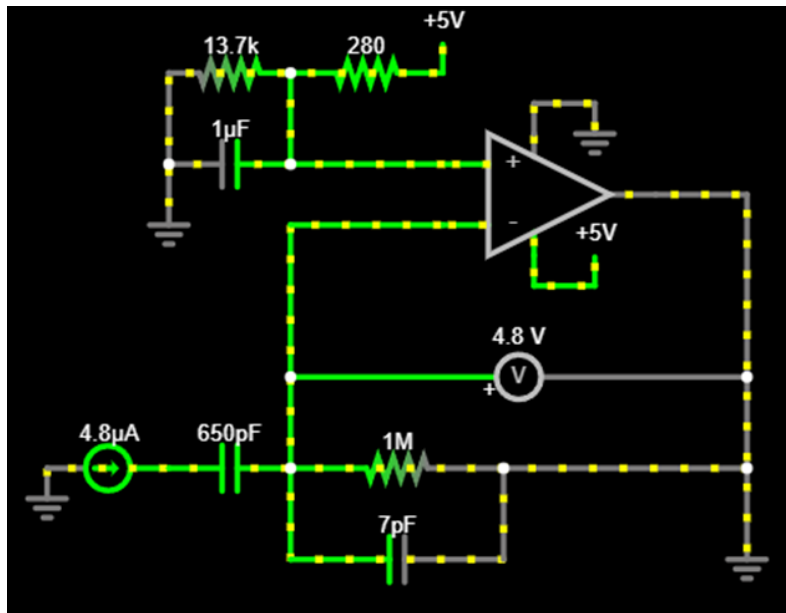
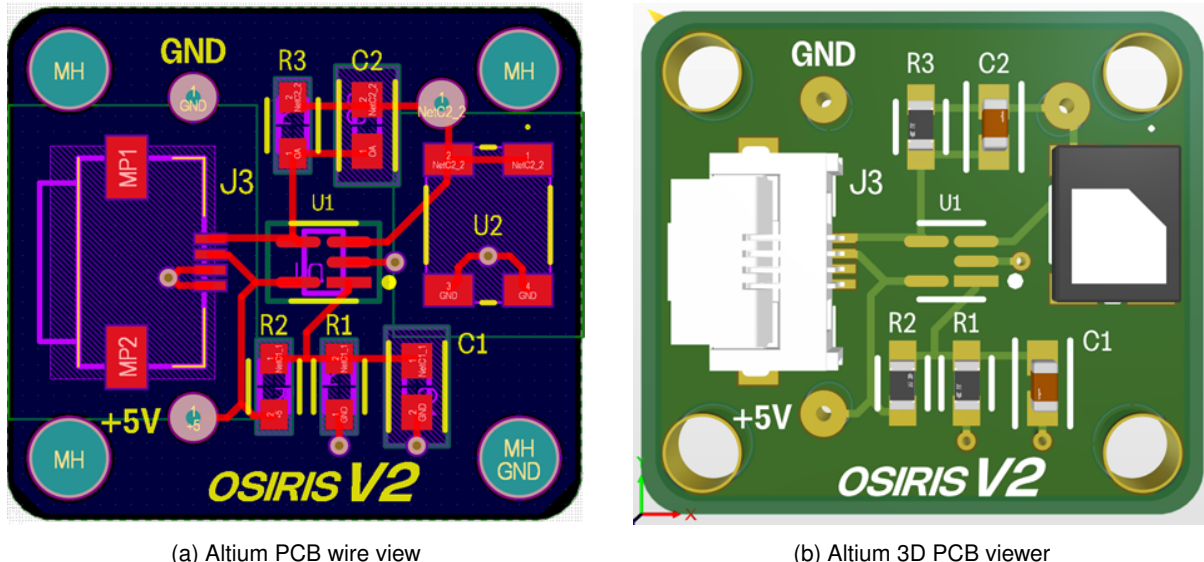


Figure 6: Falstad simulation of the OSIRISv2 module

### 5.3 PCB Design

*Please note that the photodiode in the following schematic is incorrect and is in the wrong orientation. The cathode should go to ground and the anode should go to the TIA*



(a) Altium PCB wire view

(b) Altium 3D PCB viewer

Figure 7: The photodiode sensor module is compartmentalised into five main sections. (i) The photodiode sensor (U2 - hidden behind the component on the 3D view), (ii) the transimpedance amplifier (U1), (iii) the feedback resistor and capacitor for the TIA (R3 and C2), (iv) the bias input for the TIA (R1, R2 and C1), and (v) the FPC connector (J3). Additionally, a test point for the photodiode current has been included (NetC2\_2), as well as M2 mounting holes in the corners. A ground plane was also included (second layer).

### 5.4 Fabrication

Initial orientation error of photodiodes led to saturated output. Also, higher-than-expected currents (up to  $50, \mu A$ ) required changing  $1, M\Omega$  resistor to  $50, k\Omega$ .

## 5.5 Sun Vector Determination Algorithm

Determining the position of a light source requires some modifications to the classical euclidian calculations. A standard and *easy* method to determining the position of a light source with three orthogonal assumes that each sensor has an ideal Lambertian response i.e.,  $I = I_0\cos(\theta)$ . We calculate the norm and identify the cartesian position of the source:

$$r = \sqrt{(I_x)^2 + (I_y)^2 + (I_z)^2}$$

$$(x, y, z) = (I_x/r, I_y/r, I_z/r)$$

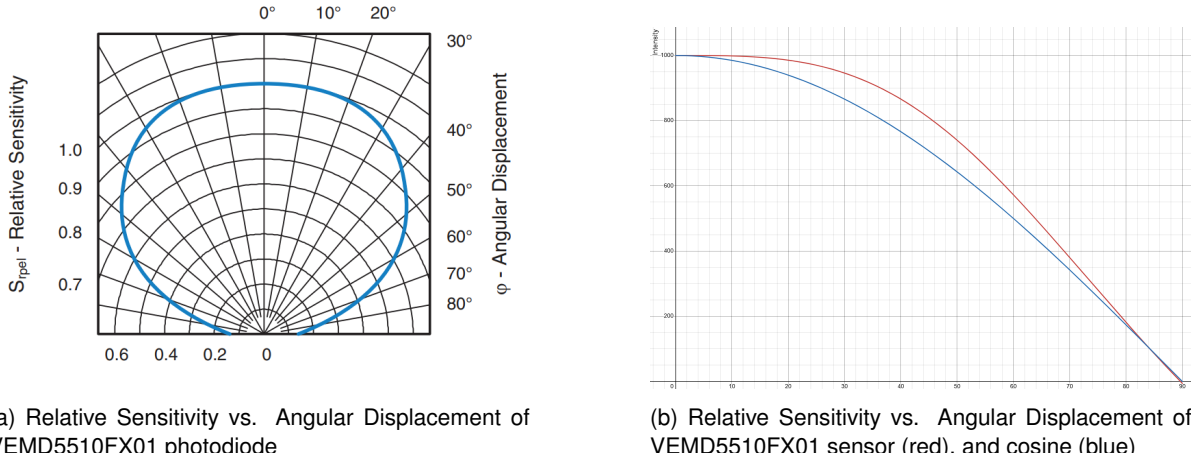
Additionally, we can determine the vector using spherical coordinates:

$$\theta = \text{atan}2(I_y, I_x)$$

$$\phi = \text{acos}(I_z, r) \quad (\zeta)$$

Where `atan2()` and `acos()` are mathematical functions in the Arduino library.

Unfortunately, the photodiodes used do not have an ideal Lambertian response, rather a polynomial response (see [8a](#)).



The aforementioned method, assuming the cosine relationship, yielded precise, but inaccurate results. The ESP32 was able to tell whether the light source was immediately in-front of one of the sensors, but greatly struggled at obtaining accurate angles once the source was moved around.

From [8b](#), we can see between  $10^\circ$  and  $75^\circ$ , there is a noticeable difference between the two functions, which agrees with the conclusion we drew from testing.

The sensor's intensity curve has been approximated to

$$f(x) = \left( \frac{1940}{1 + \left( \frac{x}{88} \right)^{3.3}} \right) - 940$$

where the input angle results in an intensity between 0 and 1. Please note that the parameters in this equation have been rounded. For the Algorithm, we will focus on the inverse:

$$x = 88 \left( \frac{1940}{f(x) + 940} \right)^{1/3.3} \quad (*)$$

When the ESP32 reads the sensor ADCs, it maps them to the desired 0-1 range where they are converted to the  $\theta$  angle using [\(\\*\)](#). From here, we can now use the previously mentioned linear algebra to determine the sun vector [\(ζ\)](#).

## 5.6 Testing

Unlike formal testing methods, OSIRISv2 utilised a studio light to simulate the sun, placed at various marked distances, heights and angles. Testing was comprised of three parts: (1) setting up the environment, (2) calibrating the sensors and (3) running the vector determination algorithm.

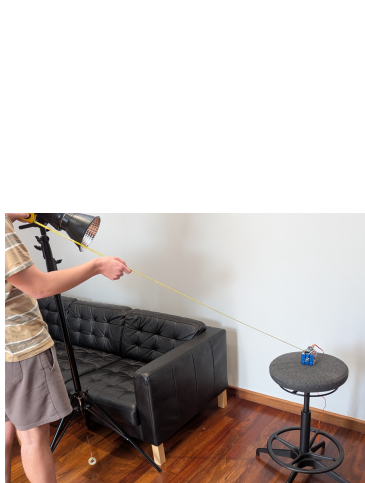
For this experiment, we used four sensor modules.

- X=1. Pointing in the +X direction.
- Y=2. Pointing in the  $\pm Y$  directions
- Z=1. Pointing in the +Z direction.

This granted us with 180° vision.

### 5.6.1 Experimental Setup

We fixed a ruler at a specific length - this will be the radial distance between OSIRIS and the studio light (see [9a](#)). We hung a plumb bob from OSIRIS and the studio light (see [9b](#)) and ensured OSIRIS was level for a correct baseline (see [9c](#)). For this experiment, OSIRIS did not change height, so we measured the height from the floor to the top sensor three times and took the median value (we measured to the top sensor and not the middle of the rubiks cube because the only calculations that use OSIRIS' vertical height involve the top sensor data and none of the side sensors).



(a) Measuring radial distance from OSIRIS to Studio Light bulb



(b) Plumb bob for OSIRIS and studio light



(c) Levelling OSIRIS platform correctly

Figure 9: Setup process for aligning the OSIRIS sensor using a plumb bob and platform levelling.

The complete set-up experiment resembled [10](#)

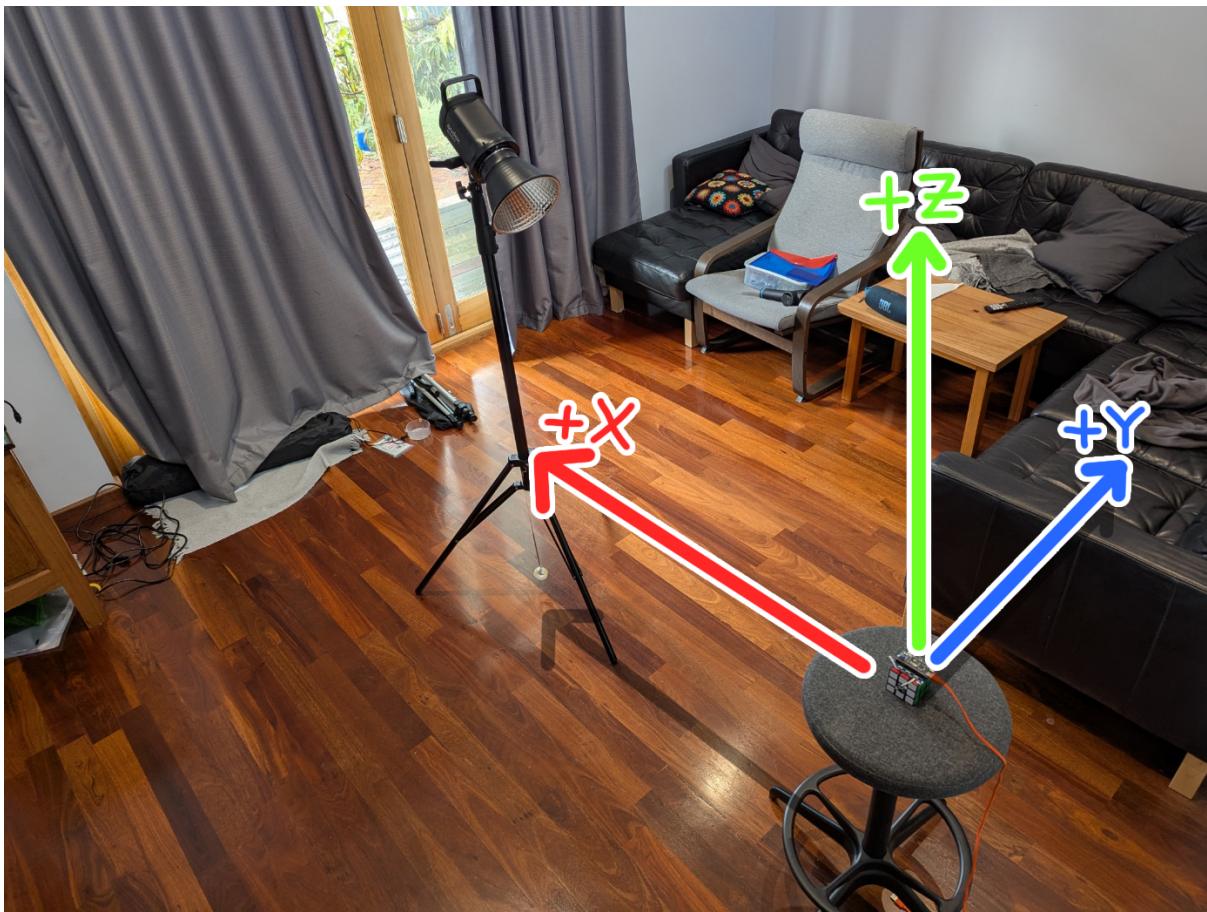


Figure 10: Annotated diagram of experimental setup. A plumb bob has been attached to the studio light. No plumb bob has been attached to the stool since the base was very close to the ground. The +X direction points towards the studio light, the +Z direction points to the sky, and +Y points to the right.

### 5.6.2 Calibration

Before the determination algorithm is run, the program first executes a calibration during the `setup()` function of the ESP32. This simultaneously reads the values from all sensors and records the minimum and maximum values for a baseline. Doing so allows the algorithm to be run in lit environments since the ambient light level will correspond to the minimum read value. This process will help produce reliable foundational data, given the vector determination algorithm is highly dependent on accurate minimum and maximum baselines.

You can now plug in the ESP32 and run the program. Calibration begins once the Serial Monitor will display the following lines:

```
Move sensors to extremes.  
→ Press and release BOOT to reset calibration values.  
→ Hold BOOT for 5 seconds and release to exit calibration.
```

This indicates the ESP32 is now in calibration mode. The light can be turned on at low power and pointed directly at OSIRIS. To calibrate the sensors, rotate OSIRIS (so there is no angle of incidence for each sensor) to record the maximum, and the ambient light levels will be used as the minimum. This process must be repeated for each distance increment since intensity drops with distance. If you believe the minimums or maximum are wrong, you can reset the values by pressing the BOOT button once, this will display the following message and restart the calibration.

Calibration values reset.

Otherwise, holding down the BOOT button for five seconds and releasing will exit calibration and proceed with the vector determination algorithm with the recorded baselines.

Calibration complete.

OSIRIS is now calibrated for that radial distance. Ensure OSIRIS' sensors are pointing in their respective directions e.g., +X in  $\phi=0^\circ$ .

### 5.6.3 Interpreting Data

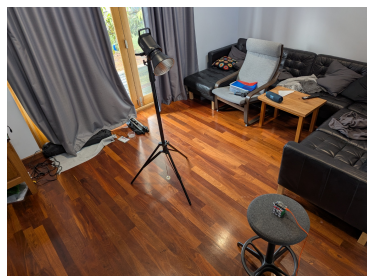
The ESP32 will now be printing the predicted vector in the Serial Monitor every 2500ms. The following is an example of what will be printed.

```
-----
Vector → X: 50, Y: 50, Z: 50
Sun Position → Azimuth: 45°, Elevation: 45°
-----
```

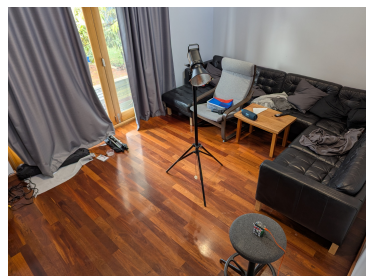
The azimuth represents the angle in the x-y plane.  $\phi = 0$  means it is pointing in the +X direction, whereas  $\phi = \pm 90$  means it is pointing in the  $\pm Y$  direction.  $\theta$  represents the angle of elevation/depression. We continued with this representation opposed to others since it was the most intuitive for the experimental set-up.

### 5.6.4 Gathering Data

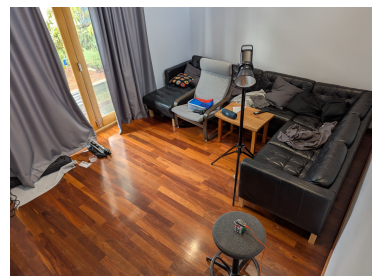
To collect data, we positioned the studio light at multiple locations around OSIRIS, maintaining a consistent radial distance between the lamp and OSIRIS as established during calibration (see 11). It was important to avoid taking big jumps between test points to ensure there were not any gaps in the data e.g., avoiding starting at 11a and moving to 11c as the second spot.



(a) Test point 1



(b) Test point 2



(c) Test point 3

Figure 11: Three examples of test points for OSIRIS testing

For every round of measurements where the studio light height was the same e.g., set at 220cm, we measured the height of the studio light to the centre of the bulb three times for increased precision and took the median value.

For every test point, we first measured the radial distance between the back of the studio light bulb and the nearest face of OSIRIS to ensure it was close to the radial distance set in 5.6.1. We then recorded the distance in the y-direction between the plumb bob and the plank that the centre of OSIRIS laid on (see 12a), and the displacement of the studio light in the Z direction (see 12b).



(a) Measuring distance in the Y direction from the plumb bob to the centre of the plank that OSIRIS was placed on



(b) Measuring the distance in the Z direction from the floor to the centre of the studio light bulb. The difference between this measurement and the height of OSIRIS was the distance in the Z direction

Figure 12: Measuring distances in the Y and Z direction for each test point

Once those measurements were complete, we recorded the values from OSIRIS into an Excel spreadsheet (see [13a](#)). The data entered into the spreadsheet for each datapoint were:

- Radial Distance (cm)
- Y Distance (cm)
- Studio Light Height (cm)
- OSIRIS Height (cm)
- OSIRIS Elevation ( $^{\circ}$ )
- OSIRIS Azimuth ( $^{\circ}$ )

The last piece of data, the z-distance, was calculated by the difference between the studio light height and OSIRIS' height. Using trigonometry, we were able to estimate the position of the studio light in spherical coordinates and compared these "real" points with OSIRIS' data. Uncertainties would be calculated from [13b](#). If the points agreed within uncertainty, we concluded that OSIRIS correctly identified the position of the studio light.

Studio Light				OSIRIS						Actual Data				Result			
R (cm)	U(R)	Y (cm)	U(Y)	Z (cm)	U(Z)	$\theta$ ( $^{\circ}$ )	U( $\theta$ )	$\phi$ ( $^{\circ}$ )	U( $\phi$ )	Z (cm)	U(Z)	$\theta$ ( $^{\circ}$ )	U( $\theta$ )	$\phi$ ( $^{\circ}$ )	U( $\phi$ )	Polar Within?	Azimuth Within?
134	6.7	0	0	142	7.1	17.5	5.00	0	5.00	103	5.2	16.92	5.00	0.00	5.00	TRUE	TRUE
129	6.5	122	6.1	142	7.1	25	5.00	81.6	5.00	103	5.2	17.60	5.00	82.82	5.00	TRUE	TRUE
133	6.7	112	5.6	142	7.1	21.7	5.00	53	5.00	103	5.2	17.05	5.00	61.74	5.00	TRUE	TRUE
143	7.2	72	3.6	142	7.1	17.7	5.00	22.8	5.00	103	5.2	15.83	5.00	31.56	5.00	TRUE	TRUE
147	7.4	37	1.85	142	7.1	15.2	5.00	6.4	5.00	103	5.2	15.39	5.00	15.13	5.00	TRUE	TRUE
146	7.3	-32	1.6	142	7.1	14.25	5.00	-5.9	5.00	103	5.2	15.49	5.00	-13.15	5.00	TRUE	TRUE
151	7.6	-84	4.2	142	7.1	12.3	5.00	-25.5	5.00	103	5.2	14.97	5.00	-35.16	5.00	TRUE	TRUE
150	7.5	-130	6.5	142	7.1	11.7	5.00	-57.7	5.00	103	5.2	15.07	5.00	-63.84	5.00	TRUE	TRUE
157	7.9	-151	7.55	142	7.1	10.7	5.00	-80.9	5.00	103	5.2	14.38	5.00	-83.17	5.00	TRUE	TRUE
150	7.5	0	0	142	7.1	12.6	5.00	0	5.00	103	5.2	15.07	5.00	0	5.00	TRUE	TRUE
154	7.7	136	6.8	175	8.75	35.7	5.00	84	5.00	103	5.2	27.87	5.00	87.4739	5.00	TRUE	TRUE
147	7.4	122	6.1	175	8.75	37.2	5.00	61.2	5.00	103	5.2	29.33	5.00	72.1635	5.00	TRUE	FALSE
150	7.5	96	4.8	175	8.75	33.1	5.00	34.2	5.00	103	5.2	28.69	5.00	46.8476	5.00	TRUE	FALSE
150	7.5	54	2.7	175	8.75	31.4	5.00	11.4	5.00	103	5.2	28.69	5.00	24.2277	5.00	TRUE	FALSE
147	7.4	0	0	175	8.75	30.5	5.00	0	5.00	103	5.2	29.33	5.00	0	5.00	TRUE	TRUE
150	7.5	-35	1.75	175	8.75	27.69	5.00	-6	5.00	103	5.2	28.69	5.00	-15.425	5.00	TRUE	TRUE
150	7.5	-72	3.6	175	8.75	29.7	5.00	-24.7	5.00	103	5.2	28.69	5.00	-33.172	5.00	TRUE	TRUE
152	7.6	-98	4.9	175	8.75	29.3	5.00	-41.2	5.00	103	5.2	28.27	5.00	-47.061	5.00	TRUE	TRUE
151	7.6	-131	6.55	175	8.75	27.8	5.00	-67	5.00	103	5.2	28.48	5.00	-80.742	5.00	TRUE	FALSE
158.5	7.9	-142	7.1	173	8.65	26.8	5.00	-84	5.00	103	5.2	26.21	5.00	-86.923	5.00	TRUE	TRUE
153	7.7	-118	5.9	200	10	43.6	5.00	-86.7	5.00	103	5.2	39.34	5.00	-85.775	5.00	TRUE	TRUE
147	7.4	-107	5.35	200	10	51.85	5.00	-67	5.00	103	5.2	41.29	5.00	-75.634	5.00	FALSE	TRUE
147	7.4	-85	4.25	200	10	50.1	5.00	-42.9	5.00	103	5.2	41.29	5.00	-50.314	5.00	TRUE	TRUE
145	7.3	-48	2.4	200	10	52.1	5.00	-17.6	5.00	103	5.2	41.99	5.00	-26.446	5.00	FALSE	TRUE
151	7.6	-73	3.65	200	10	47.15	5.00	-26.2	5.00	103	5.2	39.97	5.00	-39.11	5.00	TRUE	FALSE
145	7.3	0	0	200	10	47.3	5.00	0	5.00	103	5.2	41.99	5.00	0	5.00	TRUE	TRUE
147	7.4	25	1.25	200	10	49	5.00	0.8	5.00	103	5.2	41.29	5.00	13.0817	5.00	TRUE	FALSE
145	7.3	54	2.7	200	10	52.3	5.00	14	5.00	103	5.2	41.99	5.00	30.0683	5.00	FALSE	FALSE
146	7.3	78	3.9	200	10	54	5.00	29	5.00	103	5.2	41.64	5.00	45.628	5.00	FALSE	FALSE
147	7.4	100	5	200	10	48	5.00	46	5.00	103	5.2	41.29	5.00	64.8715	5.00	TRUE	FALSE
150	7.5	112	5.6	200	10	50	5.00	63	5.00	103	5.2	40.29	5.00	78.2049	5.00	TRUE	FALSE

(a) Data entered into Studio Light and OSIRIS columns would automatically populate the Actual Data and determine if the data points agreed within uncertainty

Uncertainty (%)	
Studio Light	Radial 5%
	Y 5%
	Z 5%
OSIRIS	$\theta$ 5
	$\phi$ 5
	Z 5%

(b) Table of uncertainties for the excel spreadsheet. Distance measurements are given in relative uncertainty and angle uncertainties are absolute

Figure 13: Excel spreadsheet for OSIRIS data

## 5.7 Analysing Results

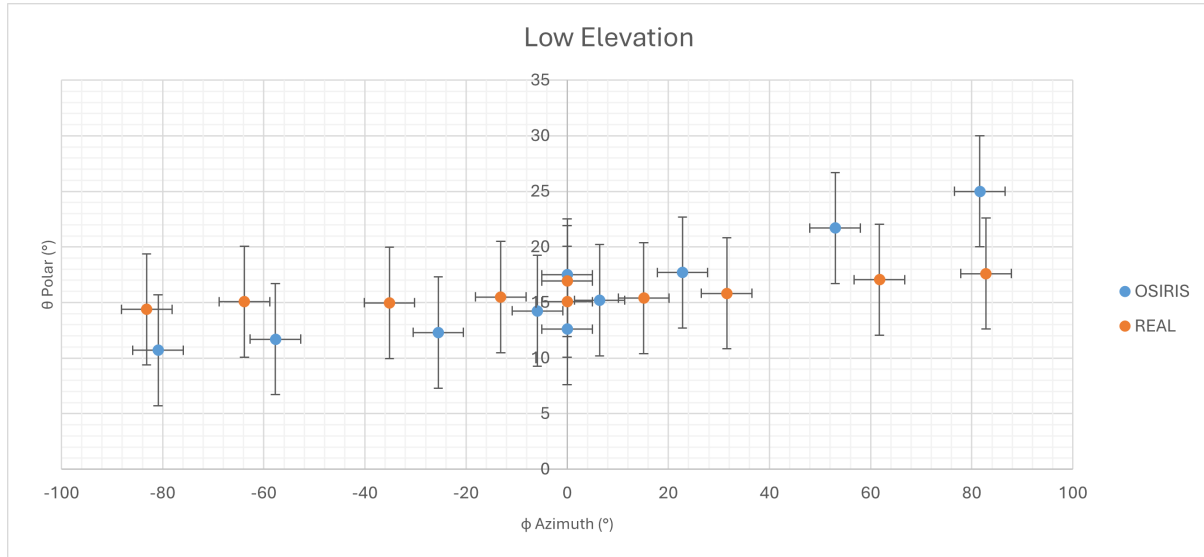


Figure 14: OSIRISv2 paired data at a low elevation with 5° of uncertainty

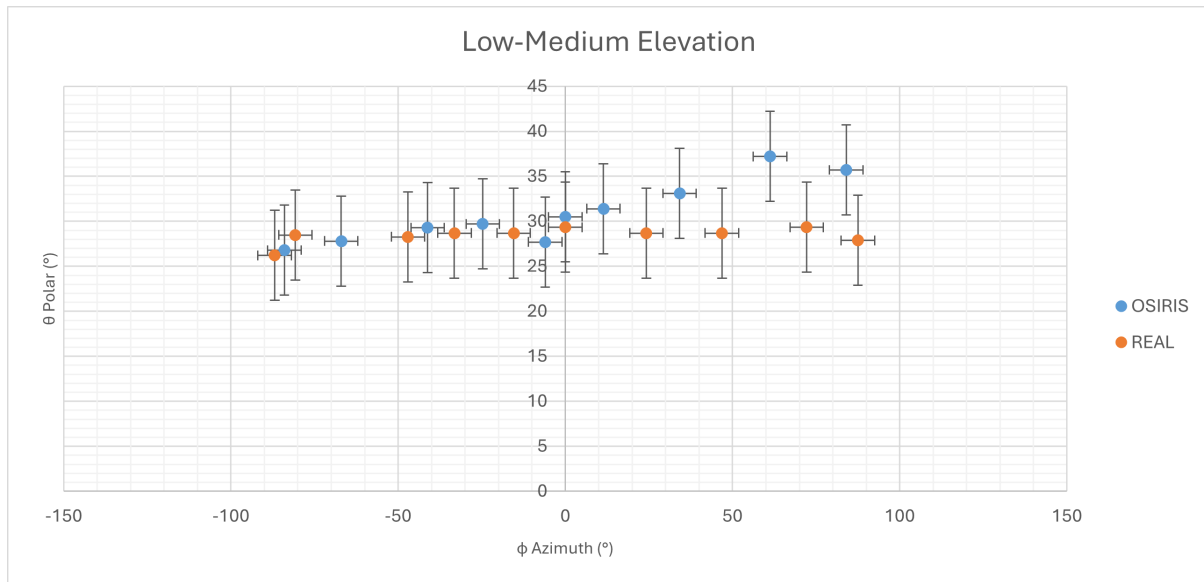


Figure 15: OSIRISv2 paired data at a low to medium elevation with 5° of uncertainty

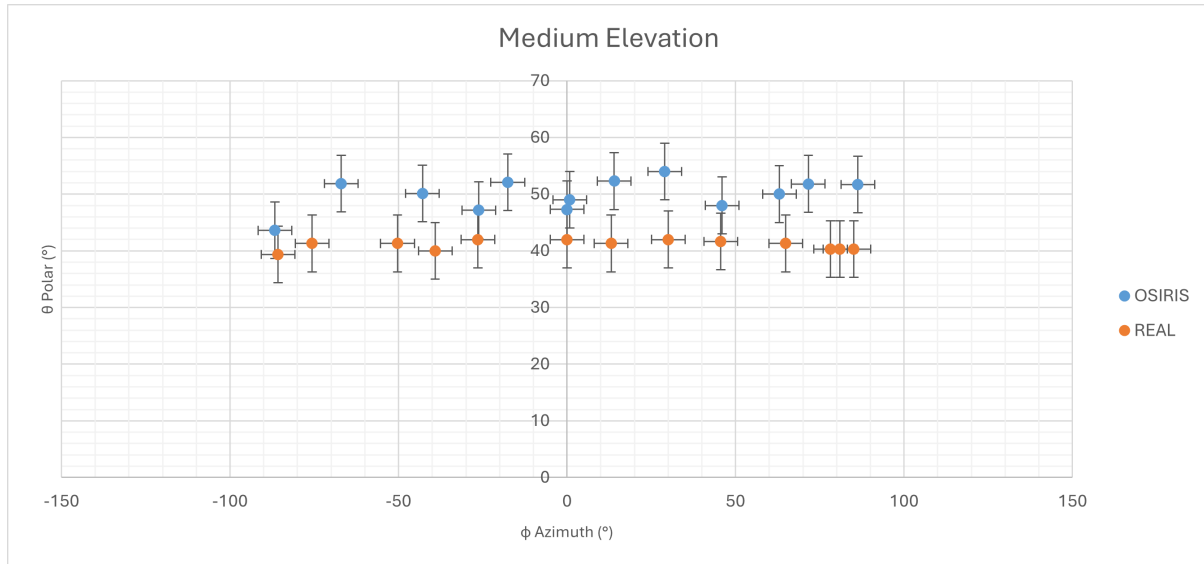


Figure 16: OSIRISv2 paired data at a medium elevation with 5° of uncertainty

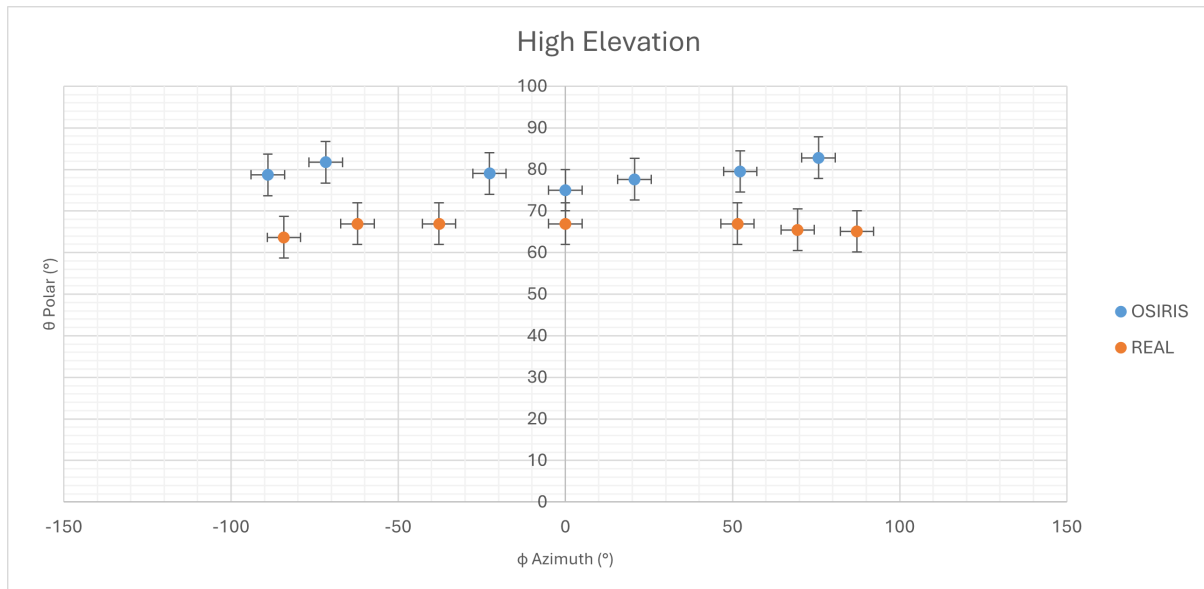


Figure 17: OSIRISv2 paired data at a high elevation with 5° of uncertainty

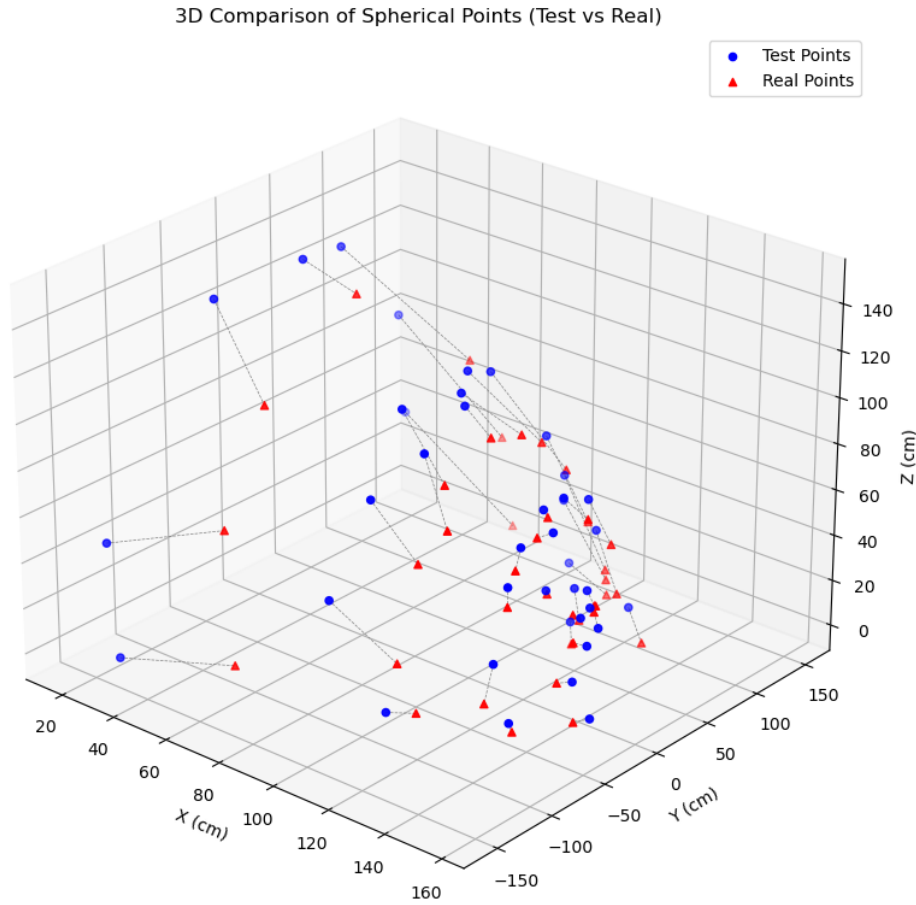


Figure 18: 3D projection of data using matplotlib

From the data presented in the above figures, it can be concluded that the OSIRIS system demonstrated excellent performance, maintaining measurement accuracy within a tight uncertainty margin of  $5^\circ$  across the majority of tested conditions. This level of precision indicates that the sensor's angular resolution and calibration are highly effective for the intended application.

Further analysis revealed that, even when considering pairs of measurements under varying conditions or sensor orientations, the results consistently agreed within a broader uncertainty range of  $10^\circ$ . This suggests good repeatability and reliability of the sensor readings across different test scenarios. Such consistency is crucial for dependable attitude determination, ensuring that OSIRIS can robustly estimate the sun vector with minimal deviation.

Overall, these findings validate the design and calibration approach of OSIRIS, highlighting its capability to provide accurate angular measurements that meet or exceed project requirements.

### 5.7.1 Uncertainties

Several sources of potential error were identified throughout the data collection and testing process:

- **Sensor Calibration:** Inaccurate or inconsistent calibration of the photodiode sensors could lead to systematic measurement errors, affecting the reliability of the collected data.
- **Radial Distance Variability:** Variations in the radial distance between the studio light and OSIRIS at different data points may introduce inconsistencies, as the incident light intensity depends on distance.
- **Measurement Errors:** Manual measurement of the heights of the studio light and OSIRIS, as well as the placement along the y-axis, is susceptible to human error and imprecision.
- **Datasheet Inaccuracies:** The photodiode datasheet contains an incorrect intensity versus angular displacement graph (Figure 8a), which may have misled interpretation or analysis of sensor response.

To mitigate these uncertainties, the development of a dedicated testing rig is proposed (see Figure 19). Such a rig would enable precise and repeatable positioning of both the sensor and the light source using

stepper motors, thereby eliminating the need for manual measurement of distances and angles. Automating the data acquisition process would not only reduce human error but also significantly increase the number of data points collected within a shorter timeframe. This approach would enhance the overall accuracy and repeatability of the testing procedure, leading to more reliable sensor characterization.

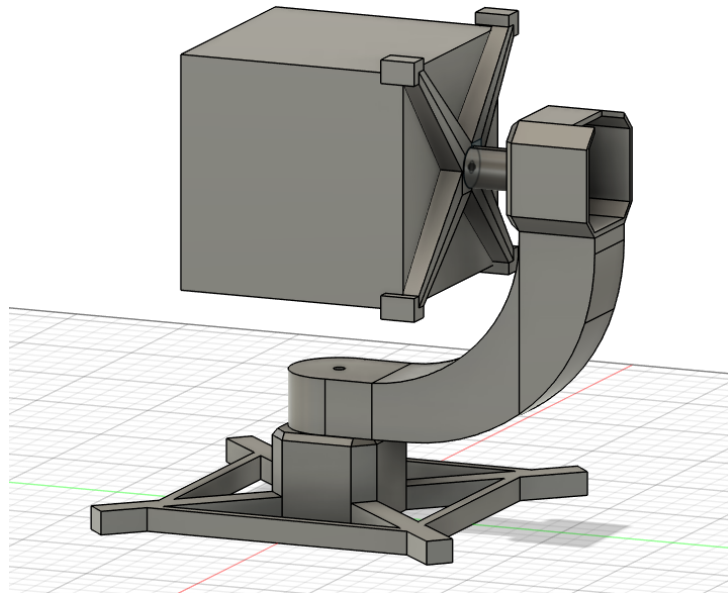


Figure 19: Prototype visualisation of the OSIRIS testing rig designed using Fusion360, illustrating the potential for automated, precise sensor and light source positioning.

## 6 Github Resources

All code and spreadsheets used for OSIRIS can be accessed through this [Github Repository](#).